Hurricane Eyewall Replacement Cycle Thermodynamics and the Relict Inner Eyewall Circulation

MATTHEW SITKOWSKI

Department of Atmospheric and Oceanic Sciences, and Cooperative Institute for Meteorological Satellite Studies, University of Wisconsin—Madison, Madison, Wisconsin

JAMES P. KOSSIN

NOAA/National Climatic Data Center, Asheville, North Carolina, and Cooperative Institute for Meteorological Satellite Studies, University of Wisconsin—Madison, Madison, Wisconsin

CHRISTOPHER M. ROZOFF

Cooperative Institute for Meteorological Satellite Studies, University of Wisconsin—Madison, Madison, Wisconsin

JOHN A. KNAFF

NOAA/NESDIS, Regional and Mesoscale Meteorology Branch, Fort Collins, Colorado

(Manuscript received 5 December 2011, in final form 7 May 2012)

ABSTRACT

Flight-level aircraft data are used to examine inner-core thermodynamic changes during eyewall replacement cycles (ERCs) and the role of the relict inner eyewall circulation on the evolution of a hurricane during and following an ERC. Near the end of an ERC, the eye comprises two thermodynamically and kinematically distinct air masses separated by a relict wind maximum, inside of which high inertial stability restricts radial motion creating a ''containment vessel'' that confines the old-eye air mass. Restricted radial flow aloft also reduces subsidence within this confined region. Subsidence-induced warming is thus focused along the outer periphery of the developing post-ERC eye, which leads to a flattening of the pressure profile within the eye and a steepening of the gradient at the eyewall. This then causes a local intensification of the winds in the eyewall. The cessation of active convection and subsidence near the storm center, which has been occurring over the course of the ERC, leads to an increase in minimum pressure. The increase in minimum pressure concurrent with the increase of winds in the developing eyewall can create a highly anomalous pressure–wind relationship. When the relict inner eyewall circulation dissipates, the air masses are free to mix and subsidence can resume more uniformly over the entire eye.

1. Introduction

A hurricane's intensity is governed by several factors including large-scale environmental conditions (e.g., vertical wind shear, sea surface temperature, and relative humidity), interactions with land, and inner-core dynamics. One specific inner-core process, an eyewall replacement cycle (ERC), is known to generate dramatic intensity and structure changes. During an ERC, a weakening, preexisting inner eyewall is replaced by an intensifying, contracting outer eyewall. This cycle often produces an oscillation of the hurricane's maximum intensity while serving as a mechanism for storm growth. These intensity and structure changes have been well studied (Willoughby et al. 1982; Willoughby 1988, 1990; Black and Willoughby 1992; Dodge et al. 1999; Hawkins et al. 2006; Houze et al. 2006, 2007; Maclay et al. 2008; Kuo et al. 2009; Sitkowski et al. 2011, hereafter SKR11; Zhou and Wang 2011; Kossin and Sitkowski 2012).

The inner core during an ERC consists of calm winds near the storm center that rapidly increase to a maximum

Corresponding author address: Matthew Sitkowski, Cooperative Institute for Meteorological Satellite Studies, University of Wisconsin—Madison, 1225 West Dayton St., Madison, WI 53706.
E-mail: matts@ssec.wisc.edu

DOI: 10.1175/MWR-D-11-00349.1

at the primary eyewall. The outer eyewall, located at a more distant radius, usually contains a secondary wind maximum with relatively enhanced vorticity, and the region between the eyewalls consists of a largely convection-free, low-vorticity moat. The region near and just inward of the primary eyewall generally contains high vorticity and is a region of enhanced inertial stability. Inertial stability is defined by $I^2 = [f + (\partial rv/r\partial r)][f + (2v/r)]$, where v is the tangential wind, r is the radius from the storm center, f is the Coriolis parameter, and $(\partial rv/r\partial r)$ is the axisymmetric vertical component of the vorticity vector. An inertially stable region provides resistance to radial motions and is an important factor in the evolution of a hurricane inner core (Schubert and Hack 1982; Hack and Schubert 1986; Kossin et al. 2000; Schubert et al. 2007; Rozoff et al. 2008; Vigh and Schubert 2009).

The demise of inner eyewall convection during an ERC is likely caused by a disruption of its transverse circulation[1] by the developing outer eyewall. Willoughby et al. (1982) and Willoughby (1988) theorized that a portion of the outer eyewall's transverse circulation moves inward toward the storm's center at upper levels and impinges on the outflow of the inner eyewall. In an alternative hypothesis, Rozoff et al. (2008) derived an analytical solution of the transverse circulation equation associated with a balanced vortex model and showed that the inertial stability of the developing outer eyewall impedes the outflow from the inner eyewall, which they hypothesized would reduce inner eyewall convection. Similarly, Rappin et al. (2011) found that weaker intensification rates occur when a storm's outflow interacts with a region of high inertial stability.

Following the demise of the inner eyewall convection, the relict inner eyewall circulation often persists as a well-defined region of high inertial stability that is resistant to horizontal mixing (Zhu et al. 2004; Chen et al. 2011), thereby impacting the local transverse circulation and potentially limiting subsidence inside the region (Schubert et al. 2007). This impacts the thermodynamic and kinematic characteristics of the eye, as well as the relationship between minimum pressure and maximum wind, toward the end of and following an ERC. This paper analyzes flight-level data to examine these impacts in detail. Section 2 briefly describes the dataset used in the study and section 3 provides an analysis of the inner-core thermodynamic changes during an ERC. Section 4 discusses the ramifications of the relict inner eyewall circulation on the kinematic, thermodynamic, and pressure structure of the inner core. A summary appears in section 5.

2. Data and methods

Aircraft flight-level data are utilized. The data, comprising kinematic and thermodynamic flight-level measurements at various isobaric levels, are described in detail by SKR11 and are briefly described here. Storm-relative tangential winds and thermodynamic data are distributed into ''radial legs'' comprising 300 0.5-km grid bins from storm center out to 150 km. One of the known sources of error in flight-level thermodynamic measurements is instrument wetting (Eastin et al. 2002). In our dataset, wetting errors are reduced following a correction outlined by Zipser et al. (1981). Remaining temperature and equivalent potential temperature (θ_e) errors, which are usually greatest in the updraft regions of the eyewall, are around 0.5°C and 2.5 K, respectively (Eastin et al. 2002). These remaining errors are small relative to the thermodynamic changes associated with ERCs, and do not substantially impact the main findings and interpretations of this paper. Further details of the flight-level data, especially regarding thermodynamic measurements, can be found in Samsury and Zipser (1995), Kossin and Eastin (2001), and Eastin et al. (2002). The best-track dataset, a record of 6-hourly storm location and intensity estimates during the entire lifetime of a tropical cyclone, is also utilized [the hurricane database (HURDAT); Jarvinen et al. 1984].

Surface pressure profiles are calculated from flight-level data in the usual manner (i.e., vertical integration of the hypsometric equation (e.g., Wallace and Hobbs 2006, 68–70). For simplicity, we assume that the mean column temperature beneath the aircraft equals the flight-level temperature (isothermal assumption). This assumption introduces a bias since the mean column temperature below the aircraft is typically warmer than the flight-level temperature, but this bias is mostly irrelevant to the main results of this study (this will be revisited briefly in section 4).

3. Thermodynamic evolution during an ERC

A climatology of intensity and structure changes during ERCs was recently completed by SKR11. They revealed that ERCs can be divided into three phases: intensification, weakening, and reintensification. During these phases, the thermodynamic structure of a hurricane inner core can undergo dramatic and highly variable changes.

Inner-core thermodynamic changes during an ERC are examined here by comparing flight-level temperature,

[1] The transverse circulation in a tropical cyclone describes the combination of radial (toward/away from storm center) and vertical (ascent/subsidence) airflow.

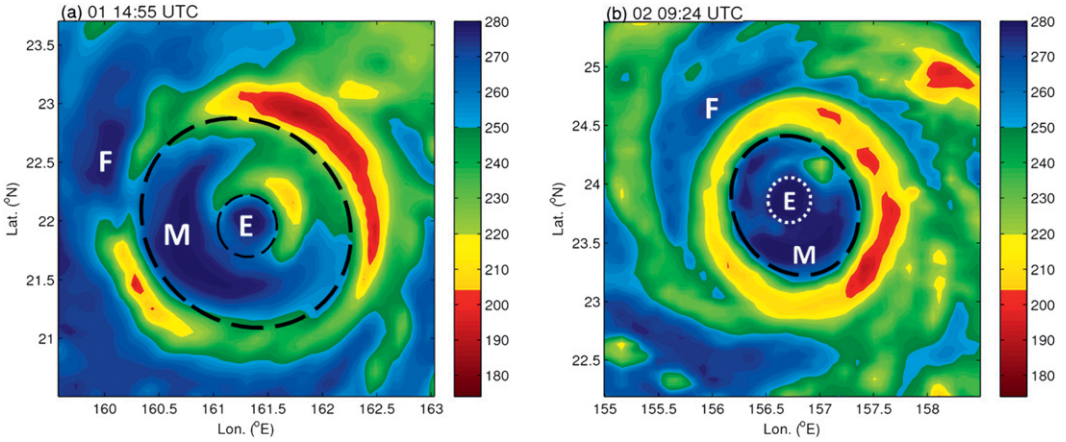

FIG. 1. Storm-centered 85-GHz imagery of brightness temperatures (K) of Hurricane Ioke (2006) taken at (a) 1455 UTC 1 Sep [Advanced Microwave Scanning Radiometer-Earth Observing System (AMSR-E)] and (b) 0924 UTC 2 Sep [Tropical Rainfall Measuring Mission Microwave Imager (TRMM-TMI)]. The typical changes in the convective presentation of the inner core during an ERC and its relationship to the three regions are shown. The letters E, M, and F represent the eye, moat, and far-field regions, respectively. The relict inner eyewall circulation (contained within the white dashed ring) and moat region together make up the developing post-ERC eye.

dewpoint, relative humidity, and θ_e at the start and end of the 24 ERCs documented by SKR11. All of the radial legs that were flown within the first and last 3 h of an ERC are divided into three regions based on flight-level measurements of tangential wind: the region from storm center to the inner wind maximum (eye), the region between the inner and outer wind maximum (moat), and the region from the outer wind maximum to the end of the radial leg (far field). Figure 1 illustrates typical changes in the convective presentation during an ERC and its relationship to these three regions. Toward the end of an ERC, the eye and moat regions together make up the newly developing eye.

The changes in the distributions of flight-level thermodynamic variables between the start and end of an ERC are shown in Fig. 2. Flight-level thermodynamic variables are highly dependent on the altitude of the aircraft, so only measurements collected at 700 hPa, the most common isobaric flight-level, are used in this analysis. When radial legs from all pressure levels are normalized through the use of a fixed tropical atmosphere sounding (e.g., Dunion and Marron 2008) and combined, the thermodynamic variables exhibit essentially the same behavior as shown in Fig. 2.

All three regions warm between the start and end of an ERC (Fig. 2a). The largest temperature increase occurs in the moat, where warming increases the mean temperature by more than 2°C (Fig. 2b). Persistent subsiding air from both eyewalls (Dodge et al. 1999; Houze et al. 2007; Rozoff et al. 2008) is likely responsible for the warming in the moat.

Dewpoint also increases significantly in all three regions between the start and end of an ERC (Fig. 2b). Dewpoint temperatures in the eye typically increase during the weakening phase of an ERC, which may be a result of a rising inversion level (Jordan 1961; Franklin et al. 1988), the ascension of a hub cloud to flight level (e.g., Schubert et al. 2007), mixing of eyewall air into the eye (Kossin and Eastin 2001), or a combination of these processes. The increase of dewpoint in the moat may be due to changes in subsidence and associated changes in inversion level, or may be due to precipitation or advective processes. Previous studies have shown that radar bright bands can exist in the moat and precipitation can be very asymmetric and intense. A radar image of Hurricane Rita (2005), for example, shows a band of high reflectivity (>30 dBZ) spiraling into a well-developed moat from the eyewall, while an echo-free region exists in a nearby portion of the moat (Didlake and Houze 2011, see their Fig. 3a).

As dewpoint temperatures increase, relative humidity in the eye and far-field regions increase significantly between the start and end of an ERC (Fig. 2c). However, mean relative humidity in the moat decreases because the temperature increase exceeds the increase of dewpoint temperatures in this region (Fig. 2c). At the end of an ERC, the relative humidity distribution of the moat is very similar to the distribution of the eye region (Fig. 2c; also cf. Houze et al. 2007). Flight-level relative humidity values in both of these regions, which together account for the total area of the developing post-ERC eye, are substantially higher than those found in the eye at the start of the ERC. It should be noted, however, that some hurricanes [e.g., Gilbert (1988) and Wilma (2005)] exhibit especially pronounced warming and drying in the

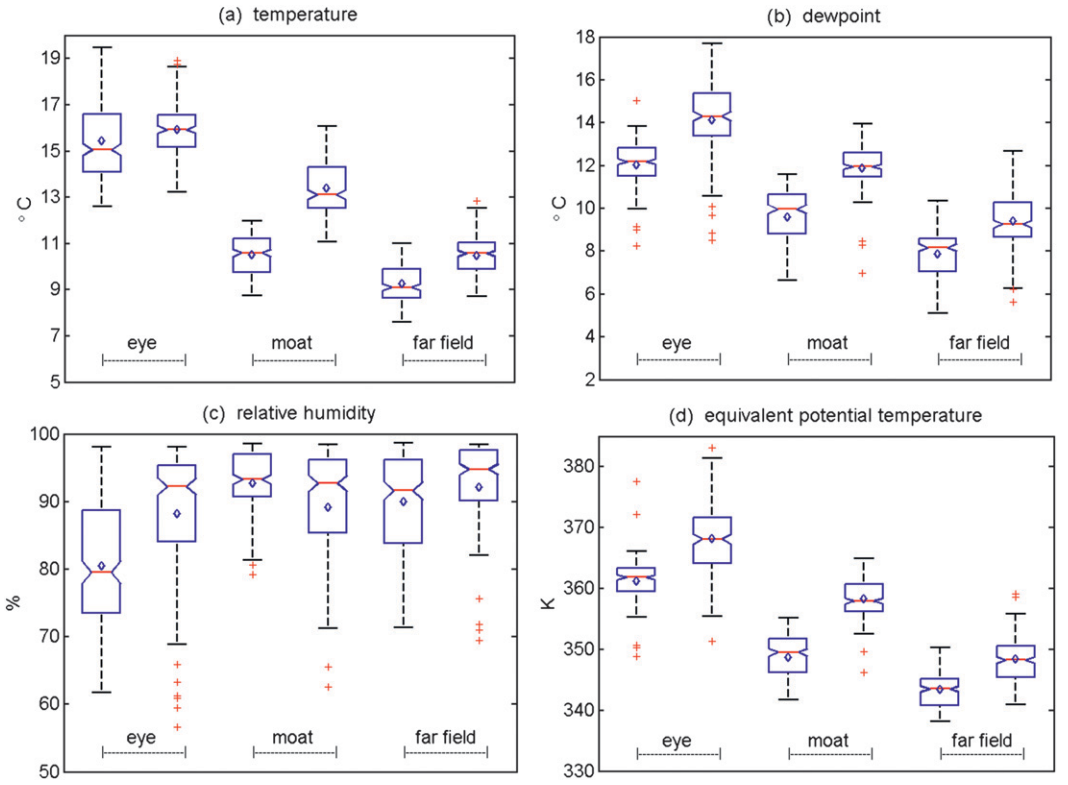

FIG. 2. Comparisons of flight-level thermodynamic data at the start and end of the 24 SKR11 ERCs. All plots are based on the mean flight-level measurements along the 700-hPa level within each region. For each region (i.e., eye, moat, and far field), the box plot on the left (right) is based on the first (last) 3 h of the ERC. The medians at the start and end of an ERC in each region are significantly different at the 5% significance level if the widths of the notches centered on the medians do not overlap. The blue diamond represents the mean of the data. Changes in flight-level (a) temperature, (b) dewpoint, (c) relative humidity, and (d) θ_e.

moat region between the inner and outer wind maxima and contain much lower relative humidity values than in the eye region. These hurricanes usually have prominent outer wind maxima forming a wall of high inertial stability early in an ERC, while inner eyewall convection is still active. This may allow for upper-level exhaust from two convectively active eyewalls to subside in the moat, generating substantial warming and drying at flight level (Rozoff et al. 2008).

Despite the similar flight-level relative humidity distributions at the end of an ERC, the eye and moat regions contain distinctly different air masses, as evident in their distributions of flight-level θ_e (Fig. 2d). The difference of their means is roughly 10 K. This difference is large enough to overcome any remaining instrumentation wetting errors and shows that two separate air masses exist in the developing post-ERC eye. This signal was observed for all of the ERCs examined by SKR11, including Hurricane Rita (2005), a case used here to illustrate a ''typical'' thermodynamic evolution of the inner core during the three ERC phases, save for the extremely dry and warm eye at the onset of the ERC (Fig. 3).

During Rita's intensification phase, the eye is warmer and drier than the rest of the inner core and two distinct θ_e maxima are located along flight level in the eyewall (Fig. 3a). A decrease of inner eyewall convection and wind speed signal the beginning of the weakening phase. In the eye, the temperature decreases and the dewpoint increases to form a θ_e maximum that is contained within the regions of high inertial stability near a radius of 20 km (Fig. 3b). An example of this warming and moistening throughout the lower troposphere, instead of one isobaric level, is shown by Houze et al. (2007, see their Fig. 3).

Temperature and dewpoint increase in the moat region as the ERC progresses (Fig. 3b). Toward the end of the ERC, warming and drying are focused along an annulus of the developing eye just inward of the outer wind maximum near 30 km (Fig. 3c). Dewpoint depressions eventually become more pronounced and expand to cover a large region of the post-ERC eye (Fig. 3d). The relevance of this selective warming and drying is discussed further in section 4.

At the end of the ERC, the air mass defining the larger, newly developing eye is not a homogenous air mass, and

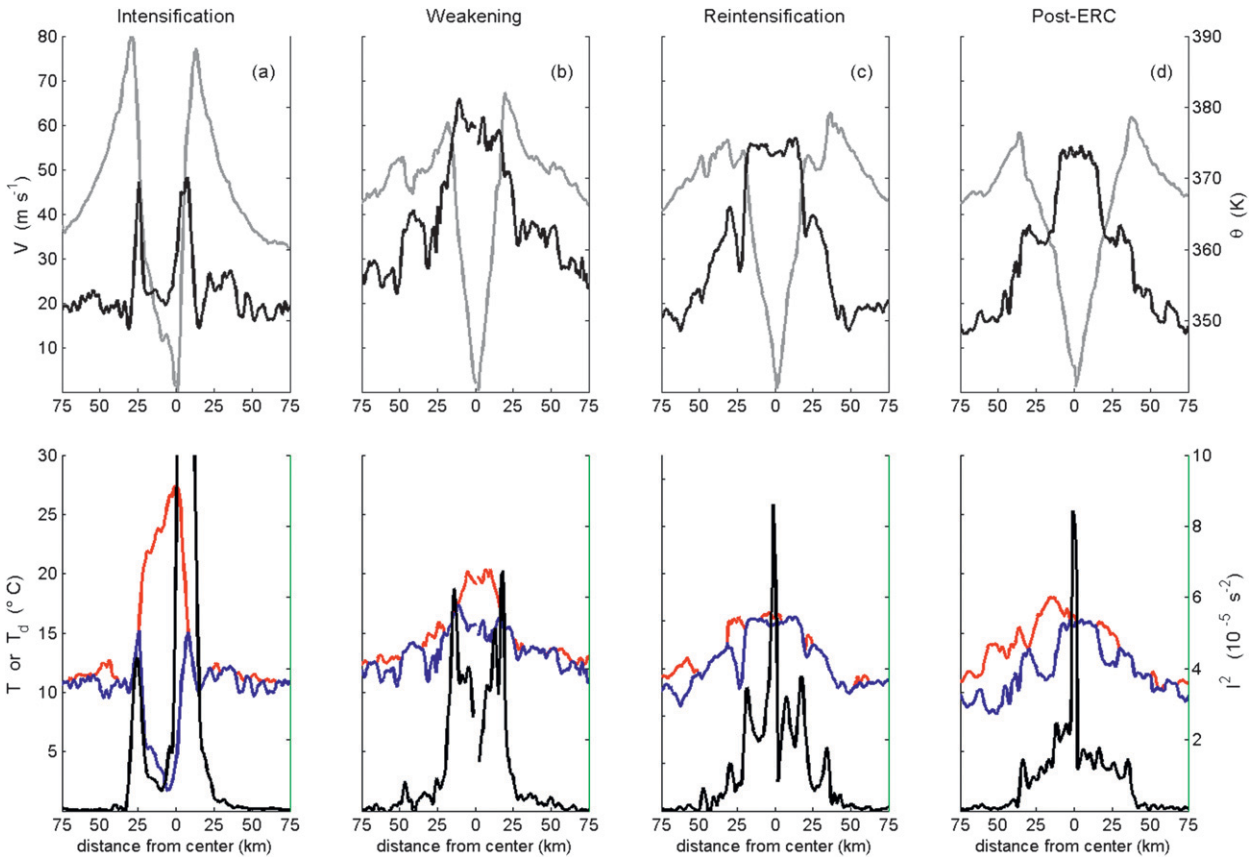

FIG. 3. Hurricane Rita (2005) flight-level measurements along the 700-hPa level from the storm center out to 75 km. (top) Tangential wind (gray) and θ_e (black). (bottom) Temperature (red), dewpoint (blue), and inertial stability (black). Measurements were taken during the (a) intensification phase at 1937 UTC 21 Sep (the inertial stability near storm center exceeds the maximum value of the y axis), (b) weakening phase at 1619 UTC 22 Sep, (c) reintensification phase at 0145 UTC 23 Sep, and (d) post-ERC period at 0600 UTC 23 Sep.

θ_e is substantially greater within the relict inner eyewall circulation than the surrounding moat (Figs. 3c,d). Since convection in the region of the inner wind maximum is largely absent during the end of the reintensification phase, θ_e is approximately conserved and serves as a useful marker for distinguishing air masses of differing origins. The θ_e increase is not gradual, but rather a sharp radial gradient exists at the inner edge of the relict inner eyewall circulation and its associated high inertial stability (Fig. 3c). In the case of Hurricane Rita, θ_e increases more than 10 K over a distance of less than 10 km inward of the relict inner eyewall circulation. This gradient defines the separation of the two air masses (i.e., the original moat and inner eye) and can persist after the completion of an ERC when the relict inner eyewall circulation can be difficult to identify in a flight-level tangential wind profile (Fig. 3d). Microwave brightness temperatures can also appear nearly uniform across the post-ERC eye (e.g., Fig. 1b).

The relict inner eyewall circulation may appear to be a desultory, insignificant feature, as it accounts for only 15% of the area in Rita's post-ERC eye (Fig. 3d), but it can have substantial ramifications on the subsequent evolution of the storm, which is the focus of the following section.

4. Ramifications of the relict inner eyewall circulation

During an ERC in Hurricane Wilma (2005), the flight-level θ_e profile exhibited a pronounced maximum near storm center on the morning of 20 October (Figs. 4a,b). The maximum was bounded by high values of inertial stability associated with the relict inner eyewall circulation (Figs. 4c,d), which forms a ''containment vessel'' that restricts horizontal motions and limits subsidence as it orbits within the larger, developing eye. The air mass within this vessel may contain the original air that was enclosed by the eyewall that developed when the storm first neared hurricane intensity, similar to the concept presented in Willoughby (1998). The moat was warm and dry, with large dewpoint depressions exceeding 7°C at this time while a large portion of the air in the relict

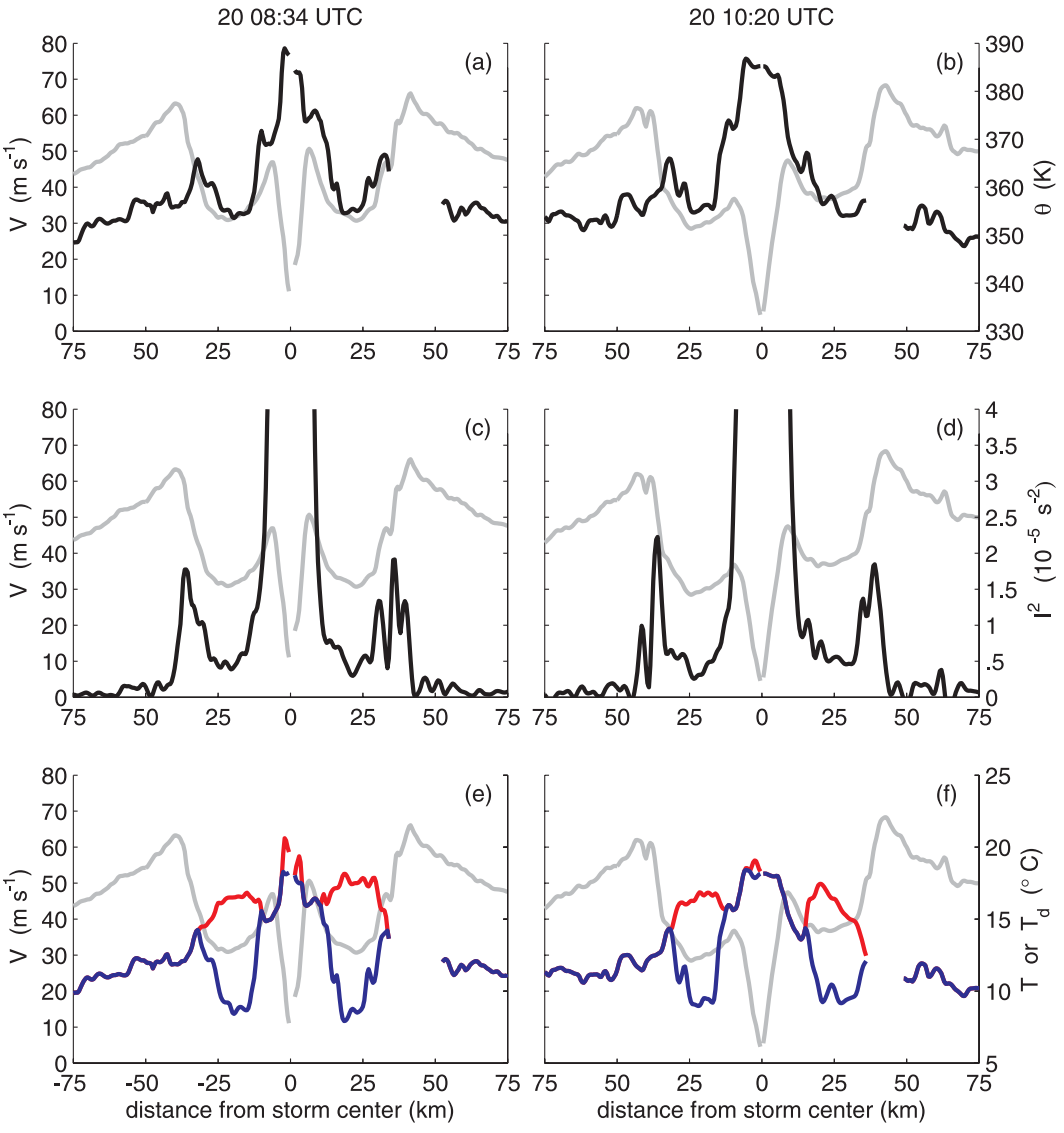

FIG. 4. Hurricane Wilma (2005) flight-level measurements along the 700 hPa level taken near (a),(c),(e) 0834 UTC 20 Oct and (b),(d),(f) 1020 UTC 20 Oct. (a),(b) Tangential wind is plotted in gray and θ_e is plotted in black. (c),(d) Tangential wind is plotted in gray and inertial stability is plotted in black. Inertial stability near storm center exceeds the maximum value of the y axis. (e),(f) Temperature, dewpoint, and tangential wind appear as red, blue, and gray lines, respectively. A small portion of thermodynamic data from 30–50 km contained large wetting errors and were removed.

inner eyewall circulation was saturated (Figs. 4e,f). This provides evidence that subsidence was strong and persistent everywhere within the developing eye except within the relict inner eyewall circulation where inertial stability was greatest. This aspect of the relict inner eyewall circulation has direct implications on both storm structure and intensity.

Figure 5 displays the evolution of the surface pressure and flight-level tangential wind profiles during the same ERC in Hurricane Wilma (2005). At 2140 UTC 19 October the tangential wind profile of the inner eyewall was very peaked and the surface pressure was very low (Fig. 5a). Nine hours later, at 0650 UTC 20 October the minimum surface pressure had risen and the inner eyewall wind speed had weakened considerably (Fig. 5b). The combination of waning convection within the inner eyewall, as evident in microwave imagery (Fig. 6), and cessation of subsidence over the inner eye likely led to reduced warming in this region and caused the minimum surface pressure to rise (Fig. 5).

Microwave imagery also indicates that the relict inner eyewall circulation was located near the outer eyewall

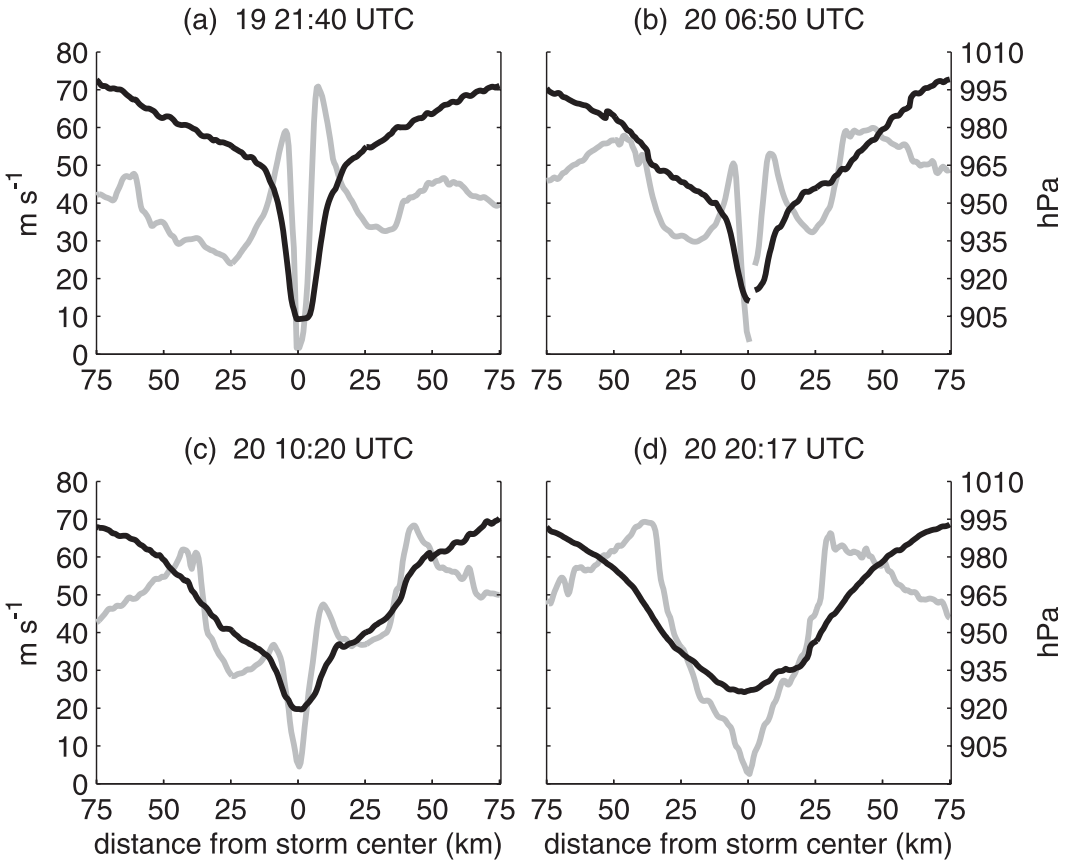

FIG. 5. Hurricane Wilma (2005) flight-level (700 hPa) tangential wind (gray line) and surface pressure (black line). The aircraft was near storm center at (a) 2140 UTC 19 Oct, (b) 0650 UTC 20 Oct, (c) 1020 UTC 20 Oct, and (d) 2017 UTC 20 Oct. As noted in the text, the actual surface pressure is likely lower than shown here.

at 1845 UTC 20 October (Fig. 6b). Visible satellite imagery (not shown) reveals that the relict inner eyewall circulation had orbited around the larger, developing eye and produced trochoidal motions of the storm center. Trochoidal motions often accompany concentric eyewall structures (Jordan 1966; Oda et al. 2006; Muramatsu 1986), as well as when only a single eyewall is present (Liu et al. 1999; Nolan et al. 2001; Marks et al. 2008; Hendricks et al. 2009). The air mass within the relict inner eyewall circulation maintained its identity and characteristics as it orbited through the much drier environment of the developing eye. This highlights the ability of the inertial stability to restrict radial motions and limit mixing between the two distinct air masses. The trochoidal orbit and longevity of the relict inner eyewall circulation exhibit similar behavior to the idealized model simulations of small offset eyes by Prieto et al. (2001).

The inertial stability within the relict inner eyewall circulation limits the transverse circulation, preventing subsidence within the relict inner eyewall circulation (Schubert et al. 2007), where the minimum pressure is located (see e.g., Kossin and Schubert 2001, their Figs. 4 and 6). Subsidence-induced warming is focused outside of the relict inner eyewall circulation, typically in an annulus along the inner periphery of the active outer eyewall convection. This warming selectively lowers surface pressure in the annulus and increases the pressure gradient just inward of the outer eyewall (Figs. 5b,c), which allows the outer eyewall to more easily contract and intensify (Willoughby et al. 1982; Shapiro and Willoughby 1982; Willoughby 1990; Vigh and Schubert 2009). The localized subsidence-induced warming also transforms the tangential wind into an increasingly U-shaped profile (Fig. 5), which produces a local vorticity maximum in the eyewall and destabilizes the local flow (Schubert et al. 1999). This can lead to dramatic rearrangements of inner-core thermodynamic and kinematic structure and subsequent changes in storm intensity (Schubert et al. 1999; Kossin and Schubert 2001, 2004; Rozoff et al. 2009; Hendricks and Schubert 2010).

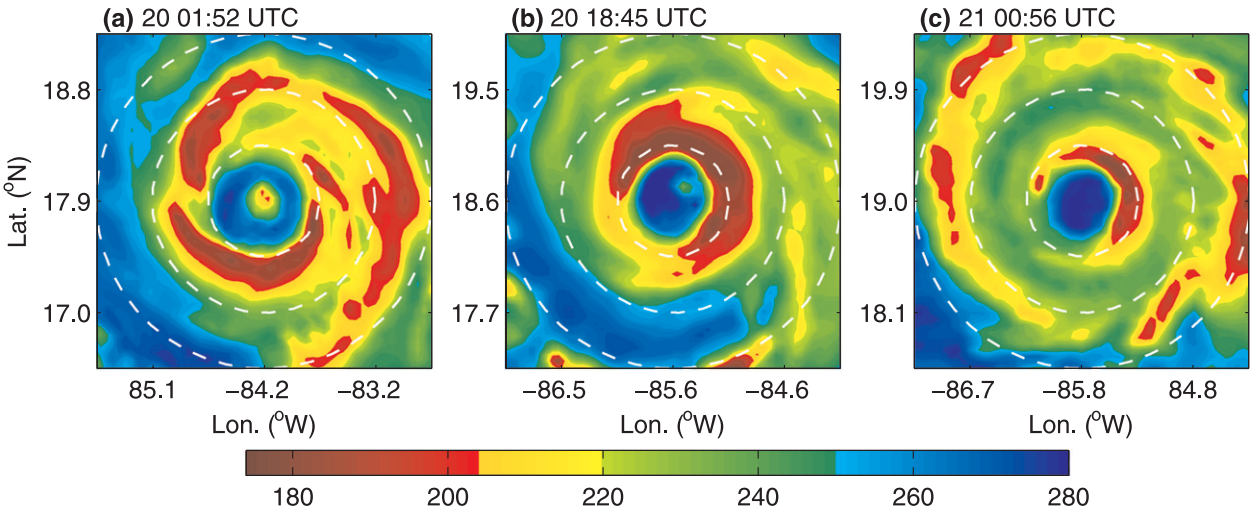

FIG. 6. 300 km × 300 km storm-centered 85-GHz imagery of brightness temperatures (K) of Wilma (2005) taken at (a) 0152 UTC 20 Oct (TRMM-TMI), (b) 1845 UTC 20 Oct (AMSR-E), and (c) 0056 UTC 21 Oct (TRMM-TMI). White range rings denote radial distances from storm center of 50, 100, and 150 km.

As mentioned previously, vertical integration of the hypsometric equation leads to a biased estimate of surface pressure under an isothermal approximation. The warmer the mean column temperature is compared to flight level, the greater the high bias. Of particular relevance here, however, is that lapse rates in the outer eyewall and moat are closer to moist and dry adiabatic, respectively, and thus the mean column temperature below flight level in the convectively active outer eyewall will be cooler than in the moat. This would have the effect of steepening the pressure gradient near the moat/outer eyewall interface even further.

The intensification of Wilma's outer eyewall winds, likely due in part to the process described above, occurred simultaneously with a steady rise of minimum pressure resulting in an anomalous pressure–wind relationship. The best-track data shows that the intensity of the storm remained at 67 m s^{-1} for 24 h (0600 UTC 20 October–0600 UTC 21 October) while the minimum pressure increased 29 hPa. The result was a highly anomalous pressure–wind relationship: 20–30 hPa lower than typically expected at the times of Figs. 5a,b (Knaff and Zehr 2007, 2008). It should be noted that the ramifications of Wilma's relict inner eyewall circulation are believed to be consistent with other storms (e.g., Fig. 3d, the region of strongly enhanced θ_e in Rita's post-ERC eye), but Wilma's anomalous pressure–wind relationship is thought to be a rather exceptional example. A detailed examination of the pressure–wind relationship specifically for Wilma was conducted by Kieu et al. (2010).

The relict inner eyewall circulation in Wilma was estimated to have dissipated around 2140 UTC 20 October (Chen et al. 2011). Shortly before this time at 2017 UTC 20 October dewpoint depressions exceeded 5°C in much of the post-ERC eye, but dewpoint values were still highest in a region of high inertial stability that was slightly offset to the right of the storm center (Figs. 7c,e). The radial legs shown in Figs. 7a,c,e occurred less than 2 h after a microwave image showed the relict inner eyewall circulation to be near the inner edge of the northeast eyewall (Fig. 6b). When aircraft sampled the inner core 14 h later, the inertial stability was greatly reduced near the storm center and the air masses in the eye had homogenized (Fig. 7d). The θ_e range across the eye was less than 5 K and the temperature and dewpoint range across the eye was less than 4°C (Figs. 7b,f). In addition, the minimum pressure recorded in the best-track decreased 4 hPa from 0600 to 1800 UTC 21 October, even though the intensity decreased 5 m s^{-1}. The pressure decrease may be an indication that subsidence had resumed over the storm center.

5. Summary

Flight-level aircraft data were used to examine the thermodynamic evolution of the inner core during an ERC, and the impact of the relict inner eyewall circulation on the evolution of the developing eye structure toward the end of and following an ERC. Flight-level temperature, dewpoint, relative humidity, and θ_e were all found to increase within the inner core over the course of an ERC, except for a decrease of mean relative humidity in the moat region. At the start of an ERC a warm, dry air mass in the eye moistens and cools as the

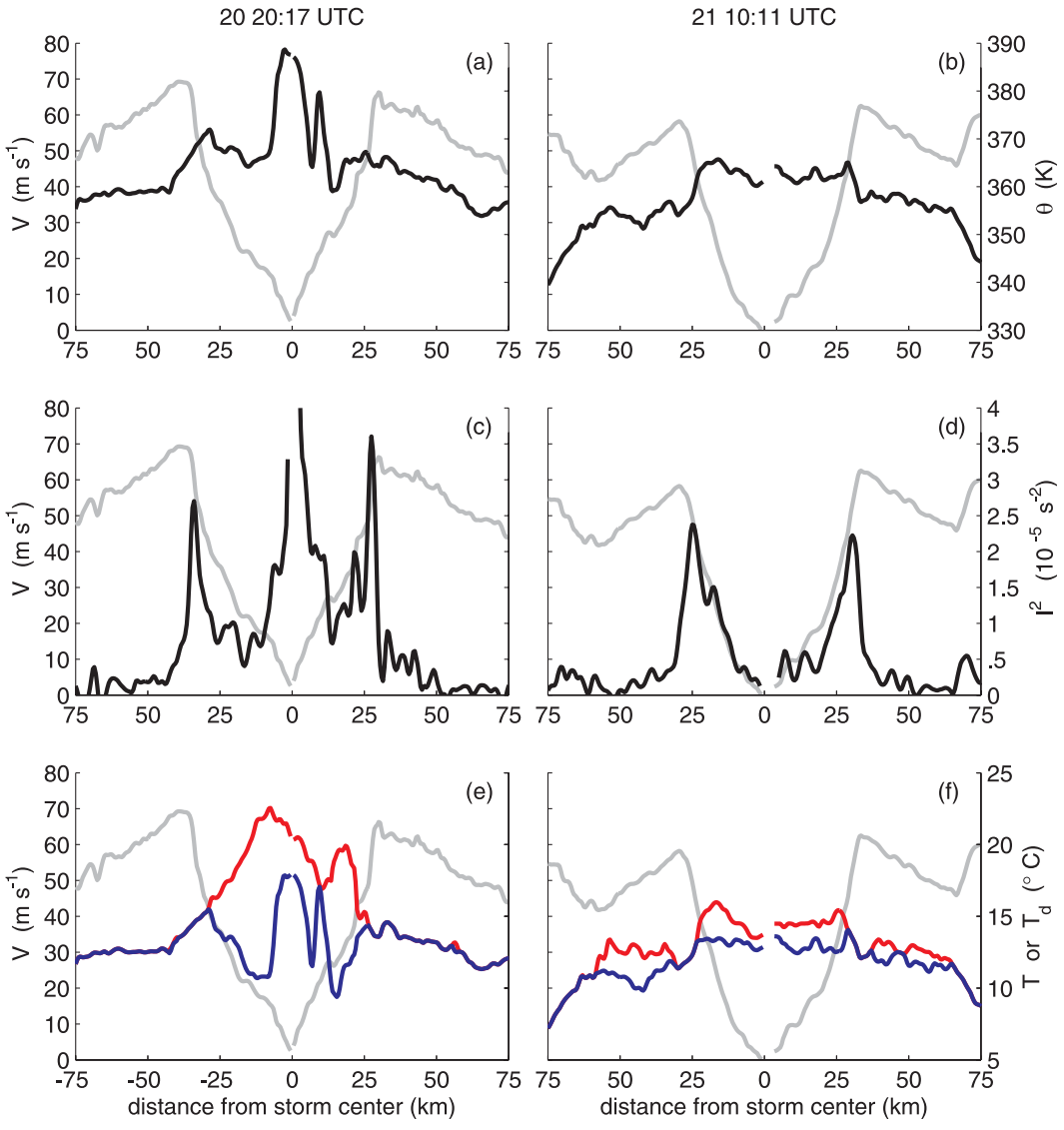

FIG. 7. As in Fig. 4, but for (a),(c),(e) 2017 UTC 20 Oct and (b),(d),(f) 1011 UTC 21 Oct.

inner eyewall weakens. This increases relative humidity significantly, such that the relative humidity in the eye is similar to values in the moat at the end of an ERC. However, a sharp radial gradient of θ_e develops near the edge of the relict inner eyewall circulation and the eye contains much higher values of θ_e, indicating that the air mass within the relict inner eyewall circulation is different than the moat air mass. This difference is still prevalent in the post-ERC eye.

The relict inner eyewall circulation produces a region of high inertial stability that constrains the transverse circulation in a developing eye and may restrict subsidence from occurring near the storm center. Large dewpoint depressions can exist in a post-ERC eye except where the old-eye air mass is encased by the high inertial stability within the relict inner eyewall circulation. Thus, subsidence-induced warming is focused in an annulus along the periphery of the developing eye. This warming steepens the surface pressure profile (i.e., increases the pressure gradient) just inward of the outer eyewall allowing it to contract (e.g., Shapiro and Willoughby 1982; Schubert and Hack 1983; Vigh and Schubert 2009) and intensify. As this occurs, waning convection around the relict inner eyewall and a lack of subsidence near the storm center reduces warming there and causes the minimum pressure to rise. This can result in an anomalous pressure–wind relationship.

The warming along the periphery of the post-ERC eye and steepening of the surface pressure profile transform the tangential wind profile into more of a U shape. This

reorganizes the vorticity of the inner core, which has implications on the barotropic instability of the eyewall, and the future evolution of the storm. Once the relict inner eyewall circulation has dissipated and the inertial stability near the storm center is reduced, pressure can decrease more uniformly throughout the region of the post-ERC eye. Thus, the relict inner eyewall circulation plays a major role in modulating the kinematic and thermodynamic structure of a post-ERC eye, and a better understanding of this feature may improve intensity forecasts. Knowledge of the relict inner eyewall circulation strength can alert forecasters on how long to expect an anomalous pressure–wind relationship and may provide insight in to the storm's intensification rate.

Acknowledgments. This work was funded by the National Oceanic and Atmospheric Administration (NOAA) through the U.S. Weather Research Program (USWRP) Joint Hurricane Testbed, the National Climatic Data Center, and National Science Foundation Grant ATM-0849689. Christopher Rozoff was supported by NOAA Geostationary Operational Environmental Satellite (GOES-R) Risk Reduction Grant NA10NES4400013. Discussion with Jonathan Vigh, Derrick Herndon, Dan Vimont, and Wayne Schubert are very much appreciated. Hua Chen and Da-Lin Zhang provided Hurricane Wilma (2005) skew *T*–log*p* diagrams that helped clarify interpretation of the analyses. We also would like to thank Matthew Eastin and an anonymous reviewer for providing helpful comments that improved the quality of the manuscript. The views, opinions, and findings contained in this report are those of the authors and should not be construed as an official National Oceanic and Atmospheric Administration or U.S. government position, policy, or decision.

REFERENCES

Black, M. L., and H. E. Willoughby, 1992: The concentric eyewall cycle of Hurricane Gilbert. *Mon. Wea. Rev.,* **120,** 947–957.

Chen, H., D.-L. Zhang, J. Carton, and R. Atlas, 2011: On the rapid intensification of Hurricane Wilma (2005). Part I: Model prediction and structural changes. *Wea. Forecasting,* **26,** 885–901.

Didlake, A. C., and R. A. Houze, 2011: Kinematics of the secondary eyewall observed in Hurricane Rita (2005). *J. Atmos. Sci.,* **68,** 1620–1636.

Dodge, P., R. W. Burpee, and F. D. Marks Jr., 1999: The kinematic structure of a hurricane with sea level pressure less than 900 mb. *Mon. Wea. Rev.,* **127,** 987–1004.

Dunion, J. P., and C. S. Marron, 2008: A reexamination of the Jordan mean tropical sounding based on awareness of the Saharan Air Layer: Results from 2002. *J. Climate,* **21,** 5242–5243.

Eastin, M. D., P. G. Black, and W. M. Gray, 2002: Flight-level thermodynamic instrument wetting errors in hurricanes. Part I: Observations. *Mon. Wea. Rev.,* **130,** 825–841.

Franklin, J. L., S. J. Lord, and F. D. Marks Jr., 1988: Dropwindsonde and radar observations of the eye of Hurricane Gloria (1985). *Mon. Wea. Rev.,* **116,** 1237–1244.

Hack, J. J., and W. H. Schubert, 1986: Nonlinear response of atmospheric vortices to heating by organized cumulus convection. *J. Atmos. Sci.,* **43,** 1559–1573.

Hawkins, J., M. Helveston, T. F. Lee, F. J. Turk, K. Richardson, C. Sampson, J. Kent, and R. Wade, 2006: Tropical cyclone multiple eyewall configurations. Preprints, *27th Conf. on Hurricanes and Tropical Meteorology,* Monterey, CA, Amer. Meteor. Soc., 6B.1. [Available online at https://ams.confex.com/ams/27Hurricanes/techprogram/paper_108864.htm.]

Hendricks, E. A., and W. H. Schubert, 2010: Adiabatic rearrangement of hollow PV towers. *J. Adv. Model. Earth Syst.,* **2,** Art. 8, 19 pp., doi:10.3894/JAMES.2010.2.8.

——, ——, R. K. Taft, H. Wang, and J. P. Kossin, 2009: Life cycles of hurricane-like vorticity rings. *J. Atmos. Sci.,* **66,** 705–722.

Houze, R. A., and Coauthors 2006: The Hurricane Rainband and Intensity Change Experiment: Observations and modeling of Hurricanes Katrina, Ophelia, and Rita. *Bull. Amer. Meteor. Soc.,* **87,** 1503–1521.

——, S. S. Chen, B. F. Smull, W.-C. Lee, and M. M. Bell, 2007: Hurricane intensity and eyewall replacement. *Science,* **315,** 1235–1239, doi:10.1126/science.1135650.

Jarvinen, B. R., C. J. Neumann, and M. A. S. Davis, 1984: A tropical cyclone data tape for the North Atlantic basin, 1886-1983: Contents, limitations, and uses. NOAA Tech. Memo. NWS/NHC 22, Miami, FL, 21 pp. [Available from National Technical Information Service, 5285 Port Royal Rd., Springfield, VA 22151.]

Jordan, C. L., 1961: Marked changes in the characteristics of the eye of intense typhoons between the deepening and filling stages. *J. Atmos. Sci.,* **18,** 779–789.

——, 1966: Surface pressure variations at coastal stations during the period of irregular motion of Hurricane Carla of 1961. *Mon. Wea. Rev.,* **94,** 454–458.

Kieu, C. Q., H. Chen, and D.-L. Zhang, 2010: An examination of the pressure–wind relationship for intense tropical cyclones. *Wea. Forecasting,* **25,** 895–907.

Knaff, J. A., and R. M. Zehr, 2007: Reexamination of tropical cyclone wind–pressure relationships. *Wea. Forecasting,* **22,** 71–88.

——, and ——, 2008: Reply. *Wea. Forecasting,* **23,** 762–770.

Kossin, J. P., and M. D. Eastin, 2001: Two distinct regimes in the kinematic and thermodynamic structure of the hurricane eye and eyewall. *J. Atmos. Sci.,* **58,** 1079–1090.

——, and W. H. Schubert, 2001: Mesovortices, polygonal flow patterns, and rapid pressure falls in hurricane-like vortices. *J. Atmos. Sci.,* **58,** 2196–2209.

——, and ——, 2004: Mesovortices in Hurricane Isabel. *Bull. Amer. Meteor. Soc.,* **85,** 151–153.

——, and M. Sitkowski, 2012: Predicting hurricane intensity and structure changes associated with eyewall replacement cycles. *Wea. Forecasting,* **27,** 484–488.

——, W. H. Schubert, and M. T. Montgomery, 2000: Unstable interactions between a hurricane's primary eyewall and a secondary ring of enhanced vorticity. *J. Atmos. Sci.,* **57,** 3893–3917.

Kuo, H.-C., C.-P. Chang, Y.-T. Yang, and H.-J. Jiang, 2009: Western North Pacific typhoons with concentric eyewalls. *Mon. Wea. Rev.,* **137,** 3758–3770.

Liu, Y., D.-L. Zhang, and M. K. Yau, 1999: A multiscale numerical study of Hurricane Andrew (1992). Part II: Kinematics and inner-core structures. *Mon. Wea. Rev.,* **127,** 2597–2616.

Maclay, K. S., M. DeMaria, and T. H. Vonder Haar, 2008: Tropical cyclone inner core kinetic energy evolution. *Mon. Wea. Rev.,* **136,** 4882–4898.

Marks, F. D., Jr., P. G. Black, M. T. Montgomery, and R. W. Burpee, 2008: Structure of the eye and eyewall of Hurricane Hugo (1989). *Mon. Wea. Rev.,* **136,** 1237–1259.

Muramatsu, T., 1986: Trochoidal motion of the eye of Typhoon 8019. *J. Meteor. Soc. Japan,* **64,** 259–272.

Nolan, D. S., M. T. Montgomery, and L. D. Grasso, 2001: The wavenumber-one instability and trochoidal motion of hurricane-like vortices. *J. Atmos. Sci.,* **58,** 3243–3270.

Oda, M., M. Nakanishi, and G. Naito, 2006: Interaction of an asymmetric double vortex and trochoidal motion of a tropical cyclone with the concentric eyewall structure. *J. Atmos. Sci.,* **63,** 1069–1081.

Prieto, R., J. P. Kossin, and W. H. Schubert, 2001: Symmetrization of lopsided vorticity monopoles and offset hurricane eyes. *Quart. J. Roy. Meteor. Soc.,* **127,** 2307–2328.

Rappin, E., M. C. Morgan, and G. Tripoli, 2011: The impact of outflow environment on tropical cyclone intensification and structure. *J. Atmos. Sci.,* **68,** 177–194.

Rozoff, C. M., W. H. Schubert, and J. P. Kossin, 2008: Some dynamical aspects of tropical cyclone concentric eyewalls. *Quart. J. Roy. Meteor. Soc.,* **134,** 583–593, doi:10.1002/qj.237.

——, J. P. Kossin, W. H. Schubert, and P. J. Mulero, 2009: Internal control of hurricane intensity variability: The dual nature of potential vorticity mixing. *J. Atmos. Sci.,* **66,** 133–147.

Samsury, C. E., and E. J. Zipser, 1995: Secondary wind maxima in hurricanes: Airflow and relationship to rainbands. *Mon. Wea. Rev.,* **123,** 3502–3517.

Schubert, W. H., and J. J. Hack, 1982: Inertial stability and tropical cyclone development. *J. Atmos. Sci.,* **39,** 1687–1697.

——, and ——, 1983: Transformed Eliassen balanced vortex model. *J. Atmos. Sci.,* **40,** 1571–1583.

——, M. T. Montgomery, R. K. Taft, T. A. Guinn, S. R. Fulton, J. P. Kossin, and J. P. Edwards, 1999: Polygonal eyewalls, asymmetric eye contraction, and potential vorticity mixing in hurricanes. *J. Atmos. Sci.,* **56,** 1197–1223.

——, C. M. Rozoff, J. L. Vigh, B. D. McNoldy, and J. P. Kossin, 2007: On the distribution of subsidence in the hurricane eye. *Quart. J. Roy. Meteor. Soc.,* **133,** 595–605, doi:10.1002/qj.49.

Shapiro, L. J., and H. E. Willoughby, 1982: The response of balanced hurricanes to local sources of heat and momentum. *J. Atmos. Sci.,* **39,** 378–394.

Sitkowski, M., J. P. Kossin, and C. M. Rozoff, 2011: Intensity and structure changes during hurricane eyewall replacement cycles. *Mon. Wea. Rev.,* **139,** 3829–3847.

Vigh, J. L., and W. H. Schubert, 2009: Rapid development of the tropical cyclone warm core. *J. Atmos. Sci.,* **66,** 3335–3350.

Wallace, J. M., and P. V. Hobbs, 2006: *Atmospheric Science: An Introductory Survey*. 2nd ed. Academic Press, 483 pp.

Willoughby, H. E., 1988: The dynamics of the tropical cyclone core. *Aust. Meteor. Mag.,* **36,** 183–191.

——, 1990: Temporal changes of the primary circulation in tropical cyclones. *J. Atmos. Sci.,* **47,** 242–264.

——, 1998: Tropical cyclone eye thermodynamics. *Mon. Wea. Rev.,* **126,** 3053–3067.

——, J. A. Clos, and M. G. Shoreibah, 1982: Concentric eyewalls, secondary wind maxima, and the evolution of the hurricane vortex. *J. Atmos. Sci.,* **39,** 395–411.

Zhou, X., and B. Wang, 2011: Mechanism of concentric eyewall replacement cycles and associated intensity change. *J. Atmos. Sci.,* **68,** 972–988.

Zhu, T., D.-L. Zhang, and F. Weng, 2004: Numerical simulation of Hurricane Bonnie (1998). Part I: Eyewall evolution and intensity changes. *Mon. Wea. Rev.,* **132,** 225–241.

Zipser, E. J., R. J. Meitin, and M. A. LeMone, 1981: Mesoscale motion fields associated with a slowly moving GATE convective band. *J. Atmos. Sci.,* **38,** 1725–1750.